

Luminescent properties of R^+ doped $Sr_2MgSi_2O_7:Eu^{3+}$ ($R^+ = Li^+, Na^+$ and K^+) orange–red emitting phosphors

Ishwar Prasad Sahu¹ · D. P. Bisen¹ · N. Brahme¹ · Raunak Kumar Tamrakar² · Ganesh Banjare¹ · Pradeep Dewangan¹

Received: 18 January 2016 / Accepted: 1 March 2016 / Published online: 9 March 2016
© Springer Science+Business Media New York 2016

Abstract $Sr_2MgSi_2O_7:Eu^{3+}$ and $Sr_2MgSi_2O_7:Eu^{3+}, R^+$ ($R^+ = Li^+, Na^+$ and K^+) phosphors were prepared by conventional solid state reaction method. The crystal structures of synthesized phosphors were an akermanite type structure which belongs to the tetragonal crystallography. The thermoluminescence kinetic parameters such as activation energy, order of kinetics and frequency factor was calculated by peak shape method. In this work, the orange-red emission originated from the ${}^5D_0-{}^7F_J$ ($J = 0, 1, 2, 3, 4$) transitions of Eu^{3+} ions could clearly be observed after samples were excited at 395 nm. Decay graph indicate that these phosphors also contain the fast and slow decay process. Mechanoluminescence intensity of prepared $Sr_2MgSi_2O_7:Eu^{3+}$ and $Sr_2MgSi_2O_7:Eu^{3+}, R^+$ ($R^+ = Li^+, Na^+$ and K^+) phosphors were increases linearly with the increasing impact velocity of moving piston (load). CIE color chromaticity diagram confirm that the prepared phosphors would emit orange-red color. Thus the present investigation indicating that this phosphor may be a potential candidate for stress sensors. The dopant R^+ ($R^+ = Li^+, Na^+$ and K^+) as charge compensator in $Sr_2MgSi_2O_7:Eu^{3+}$ can further enhance luminescence intensity, and the emission intensity of $Sr_2MgSi_2O_7:Eu^{3+}$ doping Li^+ is higher than that of Na^+ or K^+ .

1 Introduction

Phosphors are widely used in emissive displays. However, all currently used phosphors still need considerable improvement, such as lower current saturation, higher efficiency, and better chromaticity [1]. Oxide phosphors (including silicate phosphors) are more chemically stable than sulfide phosphors under high Coulomb loading. Metal silicates have been widely reported as promising host materials for rare earth and transition metal ions with excellent luminescence properties in the blue, green and red spectral regions [2]. A strontium silicate phosphor would be ideal from the manufacturing point of view, because both strontium and silica are abundant and are relatively inexpensive. These materials are widely used in the illumination, the displays, storage devices, medical instruments and many more [3, 4].

Rare earth oxides (RE_2O_3) are the most stable rare earth compounds, in which the rare earth ions hold typically a trivalent state [5]. Rare earth oxides have been widely used in the field of luminescent devices, optical transmission, bio-chemical probes, medical diagnosis and so for, because of their optical, electronic and chemical properties resulting from their 4f electrons [6, 7]. Inorganic compounds doped with trivalent europium cations (Eu^{3+}) are used for many different applications. The luminescence properties of Eu^{3+} ions involve intra 4f⁶ (4f–4f) transitions mechanisms between excited state to ground state [8, 9]. The emission wavelength of the 4f–4f transition of Eu^{3+} is relatively insensitive to the host and temperature because the 4f shell is shielded by the outer filled 5s and 5p shells. Eu^{3+} ions are employed in luminescent devices such as fluorescent lamps and cathode ray tubes [10]. Currently transitions of Eu^{3+} ions have attracted considerable interest owing to the attempt to develop novel phosphors that can

✉ Ishwar Prasad Sahu
ishwarprasad1986@gmail.com

¹ School of Studies in Physics and Astrophysics, Pt. Ravishankar Shukla University, Raipur, C.G. 492010, India

² Department of Applied Physics, Bhilai Institute of Technology, Durg, C.G. 491001, India

improve the color temperatures and the color rendering index of white light emitting diode (WLED) [11].

Recently, WLEDs are expected to replace conventional incandescent and fluorescent lamps in the near future because of their benefits in terms of high brightness, reliability, long life time, low environmental impact and energy saving. At present, the common way for manufacturing WLEDs is to combine a blue LED with $\text{Y}_3\text{Al}_5\text{O}_{12}:\text{Ce}^{3+}$ phosphor [12]. Although this type of WLEDs has a high luminous efficiency, it still reveals a low color rendering index because of deficiency in red light component [13, 14]. Thus, it is needed to develop more efficient red or orange-red emitting phosphors suitable for the fabrication of WLEDs.

Mechanoluminescence (ML) is the emission of phosphors caused by the application of mechanical energy to a solid. It can also be excited by thermal shocks caused by drastic cooling or heating of materials or by the shock waves produced during exposure of samples to laser pulses or ultrasonic waves. ML also appears during the deformation caused by the phase transition or growth of certain crystals as well as during separation of two solids in contact. ML has been observed in insulators, semiconductors as well as in conductors [15].

ML has found various important applications such as impact sensors in spacecrafts (the emission intensity can be used to determine the kinetic energy of impact), fracture sensor, damage sensor, stress sensor for the visualizations of stress field near the crack-tip, stress distribution in the solids, and quasidynamic crack-propagation in solids etc. Thus, many researchers have been focused on the investigation of phosphors with high ML. At the same time, the high stabilities, such as resistance of water, thermal stability are also very important for the application of ML. More ML phosphors with strong ML intensity and high stability are needed [16].

Therefore, in the present work, we report the phosphor synthesis, structural characterization and luminescence properties of $\text{Sr}_2\text{MgSi}_2\text{O}_7:\text{Eu}^{3+}$ and $\text{Sr}_2\text{MgSi}_2\text{O}_7:\text{Eu}^{3+}$, R^+ phosphors by solid state reaction method. Investigation on the crystal structure was determined by the X-ray diffraction (XRD) techniques. Luminescence properties were also investigated on the basis of thermoluminescence (TL), photoluminescence (PL), CIE color coordinates, decay and mechanoluminescence (ML) studies.

2 Experimental

2.1 Phosphor synthesis

The $\text{Sr}_2\text{MgSi}_2\text{O}_7:\text{Eu}^{3+}$ and $\text{Sr}_2\text{MgSi}_2\text{O}_7:\text{Eu}^{3+}$, R^+ ($\text{R}^+ = \text{Li}^+$, Na^+ and K^+) phosphors were prepared by the traditional high temperature solid state reaction method. The

starting materials were strontium carbonate [SrCO_3 (99.90 %)], magnesium oxide [MgO (99.90 %)], silicon dioxide [SiO_2 (99.99 %)] and europium oxide [Eu_2O_3 (99.90 %)], all of analytical grade (A.R.), were employed in this experiment. The contributions of Eu_2O_3 elements in the $\text{Sr}_2\text{MgSi}_2\text{O}_7:\text{Eu}^{3+}$ and $\text{Sr}_2\text{MgSi}_2\text{O}_7:\text{Eu}^{3+}$, R^+ phosphors were 3 mol%. Boric acid (H_3BO_3) was added as flux. The small amounts of flux, improve the phosphors long afterglow, luminescent intensity, reduce the phosphors synthetic temperature, improve the phosphor synthetic quality and increase the production rate. Appropriate amounts of Li_2CO_3 , Na_2CO_3 and K_2CO_3 were added as the charge compensator for Eu^{3+} doped samples. The contributions of Li_2CO_3 , Na_2CO_3 and K_2CO_3 elements in the $\text{Sr}_2\text{MgSi}_2\text{O}_7:\text{Eu}^{3+}$, R^+ phosphors were 3 mol%. Stoichiometrical amount of the raw materials was thoroughly mixed for 2 h using the mortar and pestle. The ground sample was placed in an alumina crucible and subsequently fired at 1200 °C for 3 h in an air. At last the nominal compounds were obtained after the cooling down of programmable furnace and products were finally ground into powder for characterizing the phosphors.

2.2 Measurement techniques

The crystal structures of the sintered phosphors were characterized by powder XRD analysis. Powder XRD pattern has been obtained from Bruker D8 advanced X-ray powder diffractometer and the data were collected over the 2θ range 10°–80°. The X-rays were produced using a sealed tube ($\text{CuK}\alpha$) radiation source and the wavelength of X-ray was 1.54060 Å. The X-rays were detected using a fast counting detector based on silicon strip technology (Bruker LynxEye detector). The crystal structure of the sample was verified with the help of Joint Committee of Powder Diffraction Standard Data (JCPDS) file. TL glow curve was recorded with the help of TLD reader 1009I by Nucleonix (Hyderabad, India Pvt. Ltd.) and the uncertainty value of the temperature was ± 1 K. Every time for the TL measurement, the quantity of the powder samples were kept fixed (8 mg). The excitation and emission spectrum was recorded on a Shimadzu (RF 5301-PC) spectrofluorophotometer using the Xenon lamp (150 W) as excitation source when measuring. The color chromaticity coordinates were obtained according to CIE 1931. The decay curves were obtained using a Perkin Elmer fluorescence spectrometer with the proper excitation under a UV lamp (365 nm). The ML measurement was observed by the home made lab system comprising of an RCA-931A photomultiplier tube (PMT). The ML glow curve can be plotted with the help of SM-340 application software installed in a computer attached with the storage oscilloscope. The thickness of the thick film is ~ 0.15 mm (pellet

form). All measurements were carried out at the room temperature.

2.3 Experimental setup for mechanoluminescence (ML) measurement

The experimental set up used for the impulsive deformation of ML was shown in Fig. 1. A load of particular mass and shape was dropped from different heights for striking the prepared $\text{Sr}_2\text{MgSi}_2\text{O}_7:\text{Eu}^{3+}$ and $\text{Sr}_2\text{MgSi}_2\text{O}_7:\text{Eu}^{3+}, \text{R}^+$ phosphors at different impact velocities. In this experiment, the mass of the dropping load was 400 g and shape of the load was cylindrical. The phosphor under study was placed on the upper surface of a transparent lucite plate and it was then covered with a thin aluminum foil and fixed with an adhesive tape. The foil reflects light and prevents scattering of the fragments during the impact of a moving piston onto the prepared phosphor [3]. This arrangement eliminates the error in the ML measurement due to the scattering of the crystallite fragments during the impact of the load onto the phosphor. The housing is made up of thick soft iron to provide shielding from light and magnetic field. The slit arrangement at the window is provided to adjust the size of the window according to the incident beam. When the phosphor placed on the lucite plate was crushed by impact of the load, light is emitted [9].

By changing the distance between the piston to be dropped and the sample placed on the lucite plate, the impact velocity (v_0) of the load could be changed from 98 to 328 cm/s, since the pulley and the guiding cylinder used were of negligible friction, the impact velocity (v_0) was taken as $\sqrt{2gh}$, where “g” is the acceleration due to gravity

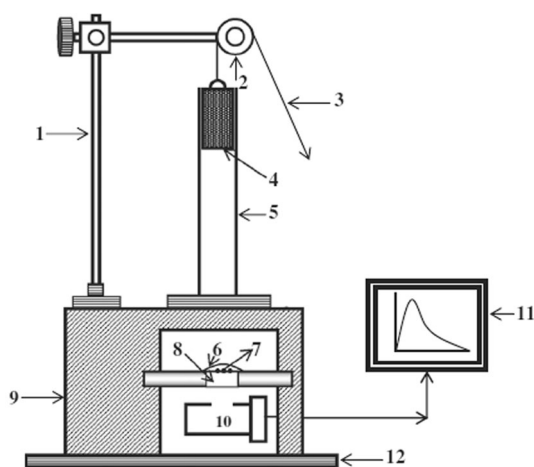


Fig. 1 Schematic diagram of the experimental setup for ML measurement

and “h” is the height through which the load is dropped freely. An RCA 931A photomultiplier tube (PMT) was placed below the transparent lucite plate [11]. The PMT was run at 750 V. The output of PMT was connected to the phosphorescent screen oscilloscope (Scientific 300 MHz, SM 340). The ML glow curve can be plotted with the help of SM-340 application software installed in a computer attached with the storage oscilloscope [13, 16].

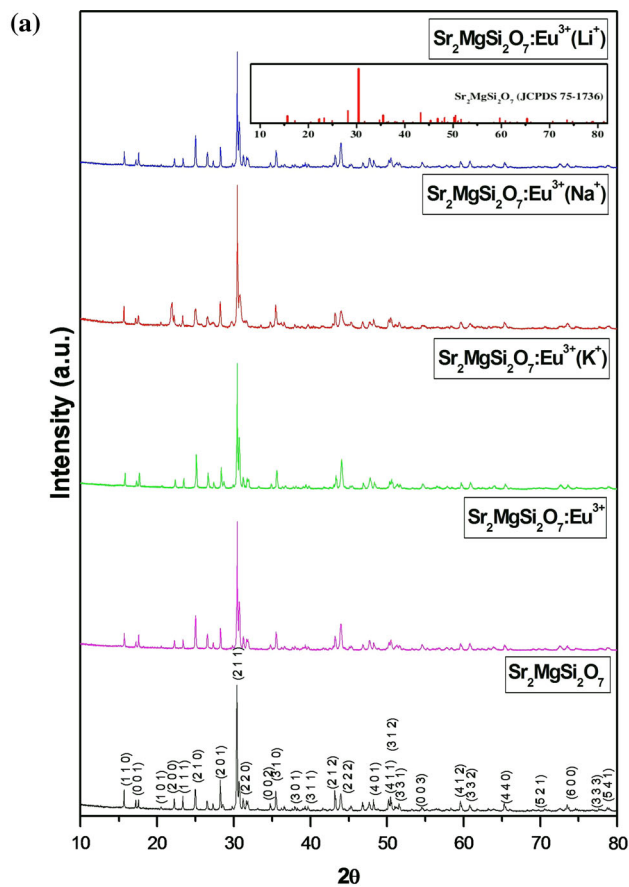
3 Results and discussions

3.1 XRD analysis

Measurements of X-ray diffraction of all powder samples were performed to verify the phase purity and to check the crystal structure. Figure 2a shows the XRD patterns of $\text{Sr}_2\text{MgSi}_2\text{O}_7$, $\text{Sr}_2\text{MgSi}_2\text{O}_7:\text{Eu}^{3+}$ and $\text{Sr}_2\text{MgSi}_2\text{O}_7:\text{Eu}^{3+}, \text{R}^+$ phosphors. All the diffraction peaks of the resultant phosphors were consistent with Joint Committee of Powder Diffraction Standard Data (JCPDS) file (JCPDS: 75-1736) [17] and all the compositions show single phase formation. No impurity phase has been observed in any of the compositions, clearly suggesting that the activator and charge compensator ions (Eu^{3+} and R^+) have been incorporated in the lattice. The dopants do not induce a significant change of the crystalline structure of $\text{Sr}_2\text{MgSi}_2\text{O}_7$ composition. Considering the effect of ionic sizes of cations, we propose that Eu^{3+} are expected to preferably occupy the Sr^{2+} (1.12 Å) sites, because of the ionic radii of Eu^{3+} (1.07 Å). The crystal of the sintered phosphor was akermanite type structure which belongs to the tetragonal crystallography with space group $\text{P}\overline{4}2_1\text{m}$ (113 space number and D_{2d}^3 space group), this structure is a member of the melilite group and forms a layered compound.

In order to obtain the crystallographic parameters of the sample, powder X-ray diffraction spectrum was analyzed by Rietveld fitting method. Figure 2b gives the comparison between observed, calculated and standard (COD card No. 96-431-7124) XRD pattern of $\text{Sr}_2\text{MgSi}_2\text{O}_7:\text{Eu}^{3+}, \text{Li}^+$ phosphor. The Standard XRD pattern of $\text{Sr}_2\text{MgSi}_2\text{O}_7$ (COD card No. 96-431-7124) seems to show quite similar pattern as observed. Figure of merit while matching observed and standard XRD pattern was 0.9409 which illustrate that phase of prepared sample agrees with the standard pattern COD card No. 96-431-7124. The pattern is characterized by few prominent peaks found at different glancing angles.

The calculated XRD pattern confirmed the presence tetragonal phase of $\text{Sr}_2\text{MgSi}_2\text{O}_7$. The indexing and refinement of lattice parameters were investigated using software Celref Version 3. The refined values of tetragonal $\text{Sr}_2\text{MgSi}_2\text{O}_7:\text{Eu}^{3+}, \text{Li}^+$ phosphor was found as; $a = 8.001 \text{ \AA}$, $b = 8.001 \text{ \AA}$, 5.1636 \AA , $\alpha = 90^\circ$, $\beta = 90^\circ$, $\gamma = 90^\circ$ and cell volume =



(b)

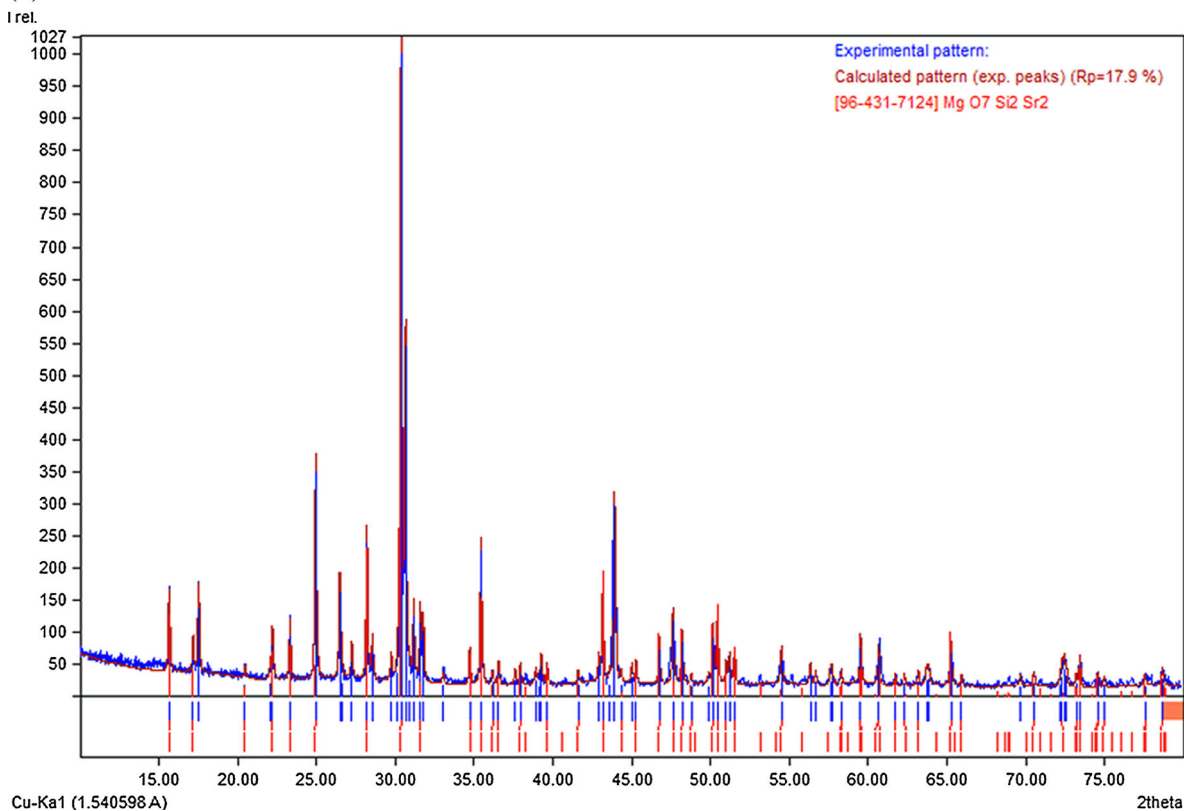


Fig. 2 a XRD patterns of $\text{Sr}_2\text{MgSi}_2\text{O}_7$, $\text{Sr}_2\text{MgSi}_2\text{O}_7:\text{Eu}^{3+}$ and $\text{Sr}_2\text{MgSi}_2\text{O}_7:\text{Eu}^{3+}$, R^+ phosphors. **b** Observed, calculated and standard XRD pattern of $\text{Sr}_2\text{MgSi}_2\text{O}_7:\text{Eu}^{3+}$, Li^+ phosphor

$332.6 (\text{\AA})^3$ which again signifies the proper preparation of the discussed $\text{Sr}_2\text{MgSi}_2\text{O}_7:\text{Eu}^{3+}$, Li^+ phosphor and is shown in Table 1.

3.2 Thermoluminescence (TL)

Thermoluminescence (TL) is a good way to detect the combination emission caused by thermal de-trapping of carriers. To get TL emission from a material three essential conditions are necessary. Firstly the material must be an insulator or a semiconductor. Secondly the material should have some time-absorbed energy during exposure to radiation. Thirdly heating the material triggers the luminescent emission. Once TL emission has been observed the material will not show it again after simply cooling the specimen and reheating it but has to be exposed to radiation to obtain TL again. What has to be emphasized is that traps and carriers (electrons and holes) may be produced by irradiation, but they are also to be created during sample processing. The plot of intensity of the emitted light against temperature is known as glow curve [18].

In order to study the trap states of the prepared $\text{Sr}_2\text{MgSi}_2\text{O}_7:\text{Eu}^{3+}$ and $\text{Sr}_2\text{MgSi}_2\text{O}_7:\text{Eu}^{3+}$, R^+ phosphors, TL glow curves were recorded and are shown in Fig. 3. The sintered phosphors were first irradiated for 10 min using 254 nm UV source, then the radiation source was removed and the irradiated samples were heated at a linear heating rate of 5 °C/s, from room temperatures to 300 °C. Initially the TL intensity increases with temperature, attains a peak value for a particular temperature, and then it decreases with further increase in temperature. A single glow peak of $\text{Sr}_2\text{MgSi}_2\text{O}_7:\text{Eu}^{3+}$ and $\text{Sr}_2\text{MgSi}_2\text{O}_7:\text{Eu}^{3+}$, R^+ phosphors were obtained at 188.42 °C, indicating that the electron traps involved are deep enough and high energy was required to release the trapped electrons; hence long storage of trapped charge carriers at normal working temperature was achieved and thus the thermal stability was ensured. The single isolated peak due to the formation of only one type of luminescence center which was created due to the UV irradiation. It is suggested that the recombination center associated with the glow at the temperature interval arises from the presence of liberated pairs, which are probably the results from the thermal release of electron/holes from electron/hole trap level and recombine at the color centers. It is also known that the doping of the rare earth ions increases the lattice defects which have

Table 1 Refined lattice parameters of $\text{Sr}_2\text{MgSi}_2\text{O}_7:\text{Eu}^{3+}$, Li^+ phosphors

Zero	Lambda	a	b	c	Alpha	Beta	Gamma	Vol.
Initial values : (refinement keys on 2nd line)								
0	1.5418	8.0107	8.0107	5.1636	90	90	90	331.4
0	0	1	0	1	0	0	0	
Final values : (standard errors on 2nd line)								
0	1.5418	8.001	8.001	5.1636	90	90	90	332.6
0	0	0.0042	0	0.0007	0	0	0	
H	K	L	2T (Obs)	2T-Zero	2Th (Cal)	Dif		
1	1	0	15.694	15.694	15.663	0.031		
1	1	1	23.36	23.36	23.3228	0.0372		
2	0	1	28.255	28.255	28.2179	0.0371		
1	2	1	30.427	30.427	30.3915	0.0355		
1	3	0	35.509	35.509	35.4786	0.0304		
2	1	2	43.24	43.24	43.2094	0.0306		
1	4	0	46.819	46.819	46.8143	0.0047		
2	2	2	47.695	47.695	47.6889	0.0061		
3	3	0	48.254	48.254	48.2564	−0.0024		
4	1	1	50.229	50.229	50.224	0.005		
3	1	2	50.502	50.502	50.5041	−0.0021		
2	1	3	59.606	59.606	59.6043	0.0017		
2	5	1	65.319	65.319	65.3555	−0.0365		
4	1	3	73.505	73.505	73.5506	−0.0456		

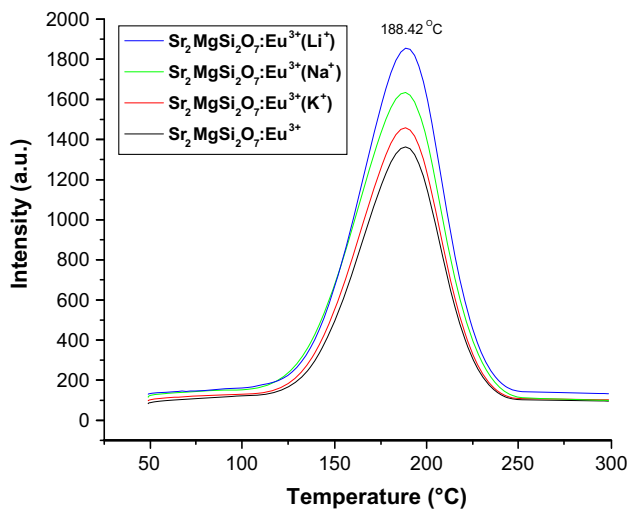


Fig. 3 TL glow curve of Sr₂MgSi₂O₇:Eu³⁺ and Sr₂MgSi₂O₇:Eu³⁺, R⁺ phosphors for 10 min UV irradiation

existed already in the host. The TL kinetic parameters were calculated and listed in Table 2.

3.3 Determination of kinetic parameters

The TL emission characteristic of a phosphor material mainly depends on the kinetic parameters describing the trapping-emitting centers which are quantitatively responsible. For example, the estimation of the time elapsed since exposure is closely related to the position of the trapping levels (E) within the band gap and frequency factor (s) of the electrons in the traps and therefore it is necessary to have a good knowledge of these parameters. There are various methods for evaluating the trapping parameters from TL glow curves [19].

Evaluation of kinetic parameters, associated with the glow peaks of the thermally stimulated luminescence, is one of the most studied subjects in the field of condensed matter physics and a complete description of the thermoluminescent characteristics of a TL material requires obtaining these parameters [20]. There are various methods for evaluating the trapping parameters from TL glow curves. For example, when one of the TL glow peaks is highly isolated from the others, the experimental method such as peak shape method is a suitable method to determine kinetic parameters. The TL parameters for the prominent glow peaks of prepared phosphor were calculated using the peak shape method [21].

3.3.1 Glow curve peak shape method

Using the glow curve peak shape method the different shape parameters of the phosphors namely the total half intensity $\omega = T_2 - T_1$ ($\tau + \delta$), τ is the half width at the low

temperature side of the peak or the low temperature half width ($\tau = T_m - T_1$); δ is the half width towards the fall-off side of the glow peak or the high temperature half width ($\delta = T_2 - T_m$), and T_m is the peak temperature and T_1 and T_2 are temperature on either side of T_m corresponding to half peak intensity were determined and presented in Table 2. Figure 4 shows the schematic diagram of glow curve peak shape method.

3.3.2 Order of kinetics (b)

The mechanism of recombination of de-trapped charge carriers with their counterparts is known as the order of kinetics (b). The order of kinetics can be predicted from shape of glow curve by using symmetry factor or geometric factor (μ_g) stated by Chen can be given as

$$\mu_g = \delta/\omega = T_2 - T_m/T_2 - T_1 \quad (1)$$

The symmetry factor is to differentiate between first and second order TL glow peak. (μ_g) = 0.39–0.42 for the first order kinetics; (μ_g) = 0.49–0.52 for the second order kinetics and (μ_g) = 0.43–0.48 for the mixed order of kinetics [22].

3.3.3 Activation energy (E)

The knowledge about trapping parameters for calculating trap information in traps centre such as required energy for escaping one electron from trap centre known as activation energy or trap depth “ E ”. So, the trap depth calculated by different methods proposed by several authors [23]. Trap depth for second order kinetics is calculated using the Eq. (2)

$$E = 2kT_m \left(1.76 \frac{T_m}{\omega} - 1 \right) \quad (2)$$

where, k is Boltzmann constant, E is activation energy; T_m is temperature of peak position.

3.3.4 Frequency factor (s)

Frequency factor reflects the probability to escape of electrons from the traps after exposure of ionizing radiation and it is one of the important parameter of the phosphor characterization. Once the order of kinetics and activation energy were determined, the frequency factor (s) can be calculated from the Eq. (3)

$$\frac{\beta E}{kT_m^2} = s \left[1 + (b - 1) \frac{2kT_m}{E} \right] \exp(E/KT_m) \quad (3)$$

where b is order of kinetics, and β is the heating rate. In the present work $\beta = 5$ °C/s.

The calculated kinetic parameters of Sr₂MgSi₂O₇:Eu³⁺ and Sr₂MgSi₂O₇:Eu³⁺, R⁺ phosphors by the peak shape

Table 2 Activation energy (E), shape factor (μ_g) and frequency factor (s^{-1}) for 10 min UV irradiated $Sr_2MgSi_2O_7:Eu^{3+}$ and $Sr_2MgSi_2O_7:Eu^{3+}, R^+$ phosphors

Phosphors name	UV Min	HTR	T_1 (°C)	T_m (°C)	T_2 (°C)	τ	δ	ω	$\mu = \delta/\omega$	Activation energy	Frequency factor
$Sr_2MgSi_2O_7:Eu^{3+}$	10	5	153.58	188.42	212.49	34.84	24.07	58.91	0.41	1.01	4.71×10^{10}
$Sr_2MgSi_2O_7:Eu^{3+} (K^+)$	10	5	154.98	188.42	212.49	33.44	24.07	57.51	0.42	1.04	9.45×10^{10}
$Sr_2MgSi_2O_7:Eu^{3+} (Na^+)$	10	5	157.58	188.42	213.46	30.84	25.07	55.91	0.45	1.07	2.18×10^{11}
$Sr_2MgSi_2O_7:Eu^{3+} (Li^+)$	10	5	157.58	188.42	212.49	30.84	24.07	54.91	0.44	1.09	3.78×10^{11}

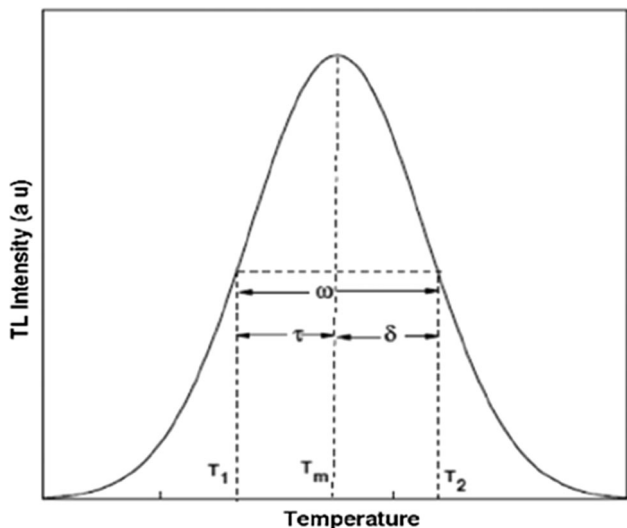


Fig. 4 Schematic diagram of glow curve peak shape method

method was given in Table 2. In our case, the value of shape factor (μ_g) was estimated to range between 0.41 to 0.45, which indicates that it is a case of mixed (intermediate) order kinetics, approaching towards second order, responsible for deeper trap depth [24], the activation energy for prepared $Sr_2MgSi_2O_7:Eu^{3+}$ and $Sr_2MgSi_2O_7:Eu^{3+}, R^+$ phosphors were >1 eV.

3.4 Photoluminescence (PL)

The excitation spectrum of $Sr_2MgSi_2O_7:Eu^{3+}$ and $Sr_2MgSi_2O_7:Eu^{3+}, R^+$ ($R^+ = Li^+, Na^+$ and K^+) phosphors were excited at 395 nm was shown in Fig. 5a. It can be seen that its emission spectra are all composed of several sharp lines from the characteristic Eu^{3+} emission. The excitation spectrum of $Sr_2MgSi_2O_7:Eu^{3+}$ and $Sr_2MgSi_2O_7:Eu^{3+}, R^+$ phosphors were exhibited a broad band in the UV region centered at about 242 nm, and several sharp lines between 300 and 400 nm. Eu^{3+} ions has a $4f^6$ configuration, it needs to gain one more electron to achieve the half-filled $4f^7$ configuration, which is relatively stable compared to partially filled configurations [25]. When Eu^{3+} is linked to the

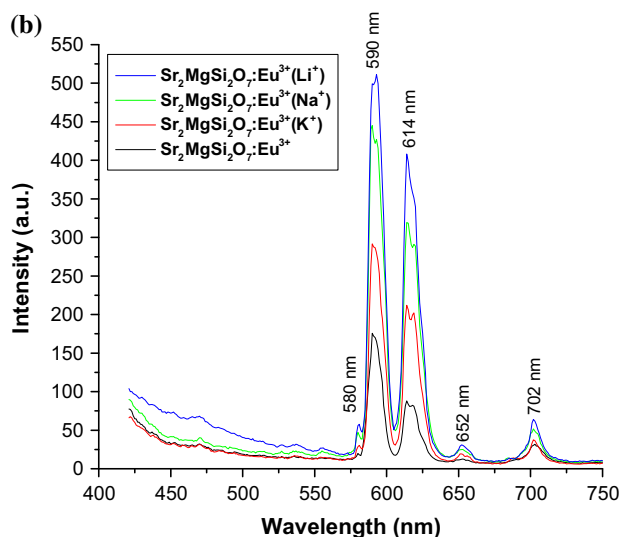
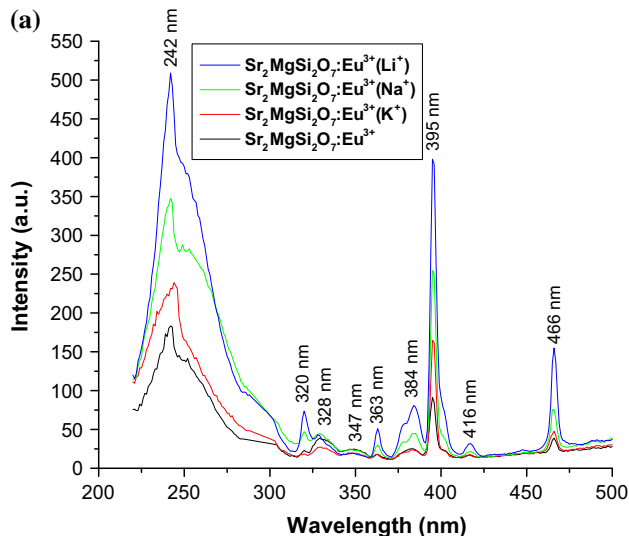


Fig. 5 a Excitation spectra of $Sr_2MgSi_2O_7:Eu^{3+}$ and $Sr_2MgSi_2O_7:Eu^{3+}, R^+$ phosphors. **b** Emission spectra of $Sr_2MgSi_2O_7:Eu^{3+}$ and $Sr_2MgSi_2O_7:Eu^{3+}, R^+$ phosphors

O ligand, there is a chance of electron transfer from O to Eu^{3+} to form $Eu^{2+}-O^2$ (simply $Eu-O$). During this, there is a broad absorption band at 230–280 nm, depending on the

host. This is known as the Eu–O charge transfer band (CTB).

It can be seen from Fig. 5a, the excitation spectrum is composed of two major parts: (1) the broad band between 220 and 300 nm, the broad absorption band is called charge transfer state (CTS) band due to the europium-oxygen interactions, which is caused by an electron transfer from an oxygen 2p orbital to an empty 4f shell of europium and the strongest excitation peak at about 242 nm. (2) A series of sharp lines between 300 and 500 nm, ascribed to the f-f transition of Eu^{3+} ions. The sharp peak is located at 395 nm corresponding to ${}^7\text{F}_0 \rightarrow {}^5\text{L}_6$ transition of Eu^{3+} . Other weak excitation peaks are located at 320, 328, 347, 363, 384, 416 and 466 nm are related to the intra-configurational 4f–4f transitions of Eu^{3+} ions in the host lattices [26]. The prepared $\text{Sr}_2\text{MgSi}_2\text{O}_7:\text{Eu}^{3+}$ and $\text{Sr}_2\text{MgSi}_2\text{O}_7:\text{Eu}^{3+}, \text{R}^+$ phosphors can be excited by near UV (NUV) at about 395 nm effectively. So, it can match well with UV and NUV-LED, showing a great potential for practical applications.

The emission spectra of $\text{Sr}_2\text{MgSi}_2\text{O}_7:\text{Eu}^{3+}$ and $\text{Sr}_2\text{MgSi}_2\text{O}_7:\text{Eu}^{3+}, \text{R}^+$ phosphors were shown in Fig. 5b in the range of 400–750 nm. Under the 395 nm excitation, the emission spectrum of our obtained samples was composed of a series of sharp emission lines, corresponding to transitions from the excited states ${}^5\text{D}_0$ to the ground state ${}^7\text{F}_j$ ($j = 0, 1, 2, 3, 4$) [27]. The orange emission at about 590 nm belongs to the magnetic dipole ${}^5\text{D}_0 \rightarrow {}^7\text{F}_1$ transition of Eu^{3+} , and the transition hardly varies with the crystal field strength. The red emission at 614 nm ascribes to the electric dipole ${}^5\text{D}_0 \rightarrow {}^7\text{F}_2$ transition of Eu^{3+} ions, which is very sensitive to the local environment around the Eu^{3+} , and depends on the symmetry of the crystal field. It is found that the 590 and 614 nm emissions are the two strongest peaks, indicating that there are two Sr^{2+} sites in the $\text{Sr}_2\text{MgSi}_2\text{O}_7:\text{Eu}^{3+}$ lattice [28]. One site, Sr(I), is inversion symmetry and the other site, Sr(II), is non-inversion symmetry. When Eu^{3+} is doped in $\text{Sr}_2\text{MgSi}_2\text{O}_7$ ions occupied the two different sites of Sr(I) and Sr(II). Other three emission peaks located at 580, 652 and 702 nm are relatively weak, corresponding to the ${}^5\text{D}_0 \rightarrow {}^7\text{F}_0$, ${}^5\text{D}_0 \rightarrow {}^7\text{F}_3$ and ${}^5\text{D}_0 \rightarrow {}^7\text{F}_4$ typical transitions of Eu^{3+} ions respectively. The strongest emission is associated to the Eu^{3+} magnetic-dipole transition of ${}^5\text{D}_0 \rightarrow {}^7\text{F}_1$, and which implies that the Eu^{3+} occupies a center of inversion asymmetry in the host lattice. For the phosphors $\text{Sr}_2\text{MgSi}_2\text{O}_7:\text{Eu}^{3+}$ and $\text{Sr}_2\text{MgSi}_2\text{O}_7:\text{Eu}^{3+}, \text{R}^+$ prepared in our experiment, the strongest orange emission peak is located at 590 nm will be dominated. It can be presumed that Eu^{3+} ions mainly occupy with an inversion symmetric center in host lattice [29]. Figure 6 shows the schematic energy level diagram of $\text{Sr}_2\text{MgSi}_2\text{O}_7:\text{Eu}^{3+}$ and $\text{Sr}_2\text{MgSi}_2\text{O}_7:\text{Eu}^{3+}, \text{R}^+$ phosphors in different emissions bands.

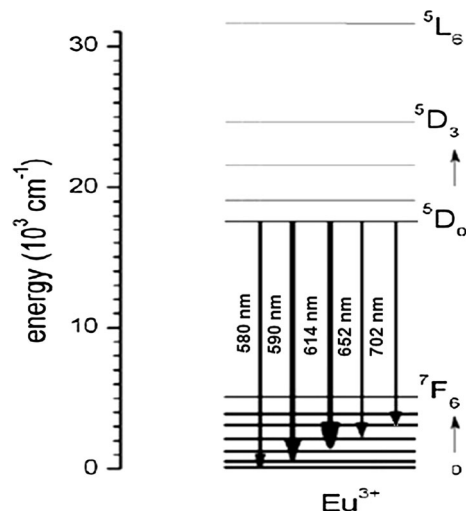


Fig. 6 Schematic energy level diagram of $\text{Sr}_2\text{MgSi}_2\text{O}_7:\text{Eu}^{3+}$ and $\text{Sr}_2\text{MgSi}_2\text{O}_7:\text{Eu}^{3+}, \text{R}^+$ phosphors

3.5 Influence of charge compensation on the luminescent intensity of $\text{Sr}_2\text{MgSi}_2\text{O}_7:\text{Eu}^{3+}$

In the $\text{Sr}_2\text{MgSi}_2\text{O}_7:\text{Eu}^{3+}$ phosphor, ions not only play the role of activator, but also act as an aliovalent auxiliary dopant to create defects. When trivalent Eu^{3+} ions is doped into the $\text{Sr}_2\text{MgSi}_2\text{O}_7$ host, Eu^{3+} substitutes chemically, but nonequivalently, in the Sr^{2+} sites. Due to these nonequivalent substitutions, an excess of positive charge in the lattice must be compensated to maintain the electroneutrality of these phosphors. There are two possible ways to realize the charge compensation. One possible way is that two Eu^{3+} ions substitute for three Sr^{2+} ions [$2\text{Eu}^{3+} + 3\text{Sr}^{2+} \rightarrow 2\{\text{Eu}_{\text{Sr}}\}^* + \{\text{V}_{\text{Sr}}\}''$], which creates two positive defects of $\{\text{Eu}_{\text{Sr}}\}^*$ and one vacancy defect of $\{\text{V}_{\text{Sr}}\}''$ with two electrons [$\{\text{V}_{\text{Sr}}\}'' \rightarrow \text{V}_{\text{Sr}} + 2e$]. The other possible charge compensation is the vacancies of Sr^{2+} [$\{\text{V}_{\text{Sr}}\}''$] created during the synthesis process. In order to improve the luminescence intensity, different charge compensation R^+ (Li^+ , Na^+ and K^+) are added to $\text{Sr}_2\text{MgSi}_2\text{O}_7:\text{Eu}^{3+}$ lattice matrix [30].

As a charge compensator ions R^+ ($\text{R}^+ = \text{Li}^+$, Na^+ and K^+) can be introduced into the host lattice of $\text{Sr}_2\text{MgSi}_2\text{O}_7:\text{Eu}^{3+}$ phosphor. The positive charge of R^+ ions neutralizes the negative charge of $\{\text{V}_{\text{Sr}}\}''$, which reduces the defects of the phosphors. Figure 5b shows the emission spectra of $\text{Sr}_2\text{MgSi}_2\text{O}_7:\text{Eu}^{3+}$ and $\text{Sr}_2\text{MgSi}_2\text{O}_7:\text{Eu}^{3+}, \text{R}^+$ ($\text{R}^+ = \text{Li}^+$, Na^+ and K^+) phosphors. It can be seen that the co-doped Li^+ , Na^+ and K^+ can all lead to the increasing luminescent intensity of Eu^{3+} ion. The reason is that Li^+ , Na^+ and K^+ occupies the site of the defects and changes the symmetry of local environment of Eu^{3+} in crystal field. The luminescence intensity can be further enhanced at Li^+

charge compensation than at Na⁺ and K⁺ charge compensation. Since Li⁺ has the least radius (0.76 Å) than Na⁺ (1.02 Å) and K⁺ (1.38 Å), it can be doped in the matrix more easily and help Eu³⁺ enter the host material effectively. Therefore, the improvement of the crystallinity caused by R⁺ ions could be another reason for the improved PL performance [31].

3.6 CIE chromaticity coordinate

In general, color of any phosphor material is represented by means of color coordinates. Color coordinates are one of the important factors for evaluating phosphors performance [31]. The luminescence color of the samples excited under 395 nm has been characterized by the CIE 1931 chromaticity diagram [32]. The emission spectrum of Sr₂MgSi₂O₇:Eu³⁺ and Sr₂MgSi₂O₇:Eu³⁺, R⁺ phosphors were converted to the CIE 1931 chromaticity using the photoluminescent data and the interactive CIE software (CIE coordinate calculator) diagram as shown in Fig. 7.

Every natural color can be identified by (x, y) coordinates that are disposed inside the ‘chromatic shoe’ representing the saturated colors. Luminescence colors of Sr₂MgSi₂O₇:Eu³⁺ and Sr₂MgSi₂O₇:Eu³⁺, R⁺ phosphors were placed in the orange-red (x = 0.523, y = 0.370), corners. The chromatic co-ordinates of the luminescence of this phosphor are measure and reached to orange-red luminescence.

3.7 Decay

Figure 8 shows the typical decay curves of Sr₂MgSi₂O₇:Eu³⁺, Li⁺ phosphor. The initial afterglow intensity of the sample was high. The decay times of phosphor can be calculated by a curve fitting technique, and the decay curves fitted by the sum of two exponential components have different decay times.

$$I = A_1 \exp(-t/\tau_1) + A_2 \exp(-t/\tau_2) \tag{4}$$

where, I is phosphorescence intensity, A₁, A₂ are constants, t is time, τ₁ and τ₂ are decay times (in ms) for the exponential components. Decay curves are successfully fitted by the Eq. (4) and the fitting curve result are shown. The results indicated that the, decay curves are composed of two regimes, i.e., the initial rapid decaying process and the subsequent slow decaying process.

As it was reported, when Eu³⁺ ions were doped into Sr₂MgSi₂O₇, they would substitute the Sr²⁺ ions. To keep electro-neutrality of the compound, two Eu³⁺ ions would substitute three Sr²⁺ ions. The process can be expressed as Eq. (5)

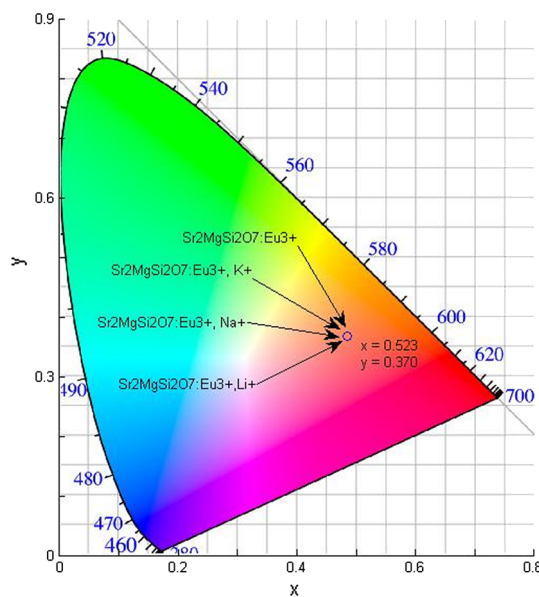
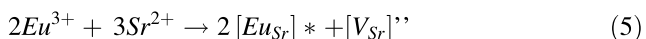


Fig. 7 CIE chromaticity diagram of Sr₂MgSi₂O₇:Eu³⁺ and Sr₂MgSi₂O₇:Eu³⁺, R⁺ phosphors

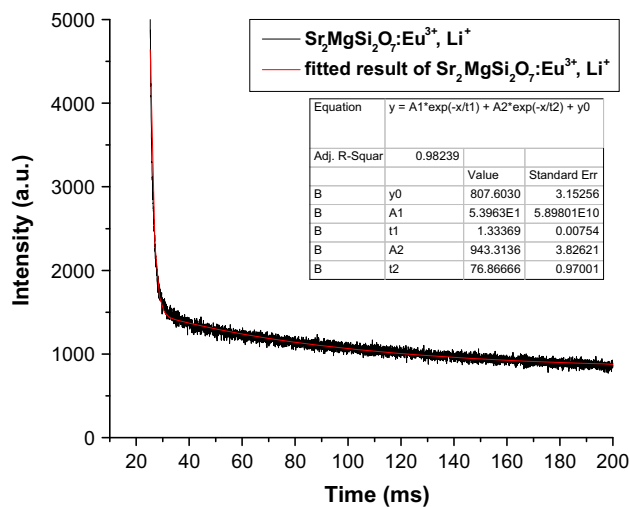


Fig. 8 Decay curves of Sr₂MgSi₂O₇:Eu³⁺, Li⁺ phosphor

Each substitution of two Eu³⁺ ions would create two positive defects of [Eu_{Sr}]^{*} capturing electrons and one negative vacancy of [V_{Sr}]^{''}. These defects act as trapping centers for charge carriers. Then the vacancy [V_{Sr}]^{''} would act as a donor of electrons while the two [Eu_{Sr}]^{*} defects become acceptors of electrons. By thermal stimulation, electrons of the [V_{Sr}]^{''} vacancies would then transfer to the Eu³⁺ sites. The results indicate that the depth of the trap is too shallow leading to a quick escape of charge carriers from the traps resulting in a fast recombination rate in milliseconds (ms) [33].

3.8 Mechanoluminescence (ML)

In the present ML studies, an impulsive deformation technique has been used. During the deformation of a solid, a great number of physical processes may occur within very short time intervals, which may excite or stimulate the process of photon emission [34]. When a moving piston was dropped onto the phosphors, initially the ML intensity increases with time, attains a peak value and then decreases with time. Such a curve between the ML intensity and deformation time of phosphors were known as the ML glow curve. It is seen that when moving piston was dropped at

particular height, then the ML emission also takes place [35]. The prepared phosphors were fracture without any pre-irradiation such as X-ray, β -rays, γ -rays, UV, etc. Every time for the ML measurement, the quantity of prepared $\text{Sr}_2\text{MgSi}_2\text{O}_7:\text{Eu}^{3+}$ and $\text{Sr}_2\text{MgSi}_2\text{O}_7:\text{Eu}^{3+}, \text{R}^+$ phosphors were kept constant (8 mg) and it was placed onto the upper surface of a transparent Lucite plate. The ML was excited impulsively by dropping a load onto the sample from different heights ($h = 10, 20, 30, 40, 50$ cm). The phosphor was fracture via dropping a load [moving piston] of particular mass (400 g) and cylindrical shape on the $\text{Sr}_2\text{MgSi}_2\text{O}_7:\text{Eu}^{3+}$ and $\text{Sr}_2\text{MgSi}_2\text{O}_7:\text{Eu}^{3+}, \text{R}^+$ phosphors. The velocity

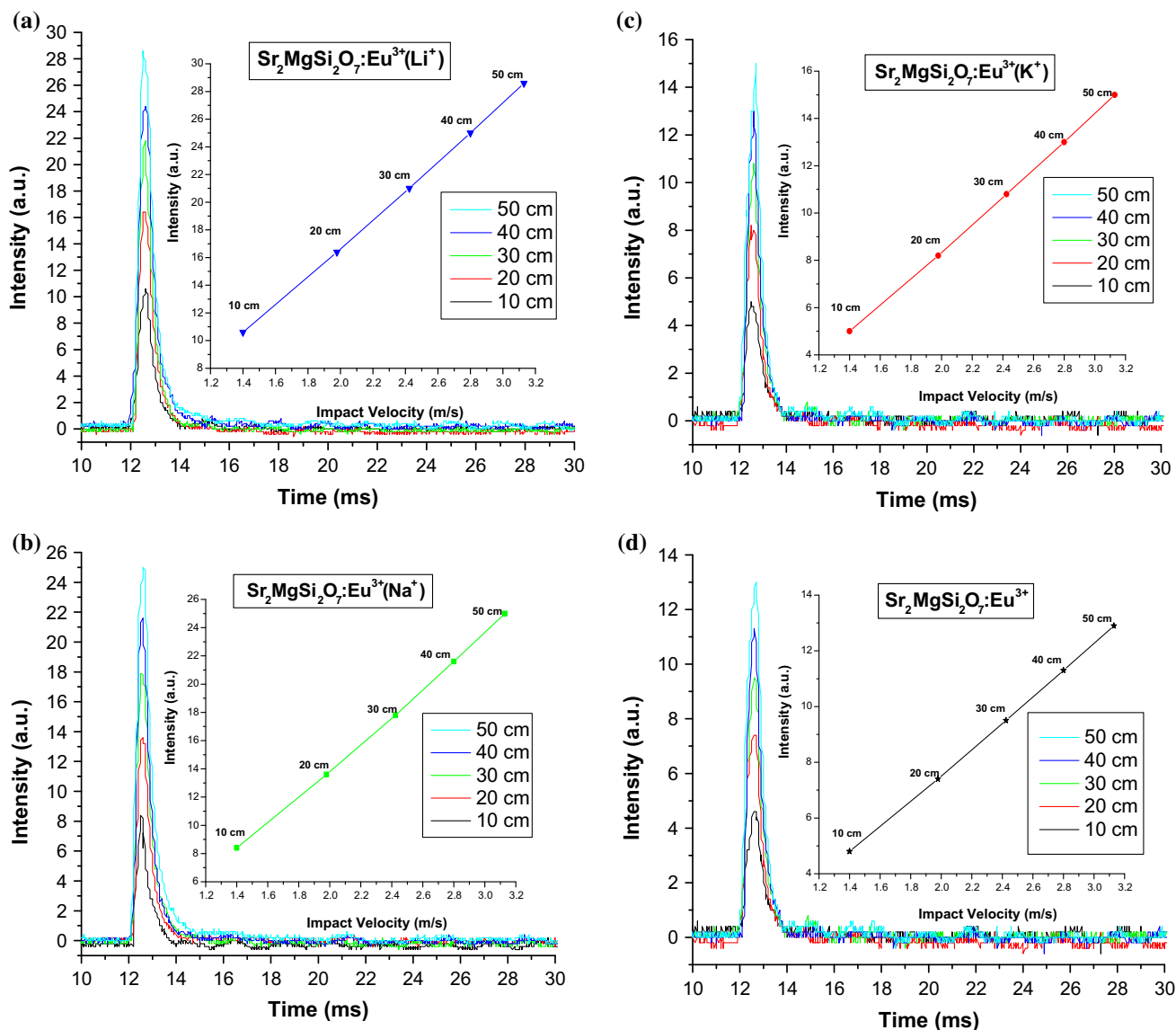


Fig. 9 a ML intensity versus time curve of $\text{Sr}_2\text{MgSi}_2\text{O}_7:\text{Eu}^{3+}$, Li^+ phosphor (inset ML intensity versus impact velocity curve of $\text{Sr}_2\text{MgSi}_2\text{O}_7:\text{Eu}^{3+}$, Li^+ phosphor). b ML intensity versus time curve of $\text{Sr}_2\text{MgSi}_2\text{O}_7:\text{Eu}^{3+}$, Na^+ phosphor (inset ML intensity versus impact velocity curve of $\text{Sr}_2\text{MgSi}_2\text{O}_7:\text{Eu}^{3+}$, Na^+ phosphor). c ML

intensity versus time curve of $\text{Sr}_2\text{MgSi}_2\text{O}_7:\text{Eu}^{3+}$, K^+ phosphor (inset ML intensity versus impact velocity curve of $\text{Sr}_2\text{MgSi}_2\text{O}_7:\text{Eu}^{3+}$, K^+ phosphor). d ML intensity versus time curve of $\text{Sr}_2\text{MgSi}_2\text{O}_7:\text{Eu}^{3+}$ phosphor (inset ML intensity versus impact velocity curve of $\text{Sr}_2\text{MgSi}_2\text{O}_7:\text{Eu}^{3+}$ phosphor)

of the moving piston, holding the impact mass, could be changed (from 140 to 313 cm/s), by changing the height through which it was dropped. Figure 9a–d shows that the characteristics glow ML curve between ML intensity versus time for different heights (impact velocity). When the moving piston was dropped onto the prepared phosphor at different height, light is emitted. The photon emission time is nearly 2 ms, when prepared phosphors fracture. In these ML measurements, maximum ML intensity has been obtained for the 50 cm dropping height and ML intensity increases with the dropping height of the moving piston. Figure 9a–d, inset shows that the characteristics curve between ML intensity versus impact velocity of $\text{Sr}_2\text{MgSi}_2\text{O}_7:\text{Eu}^{3+}$ and $\text{Sr}_2\text{MgSi}_2\text{O}_7:\text{Eu}^{3+}$, R^+ phosphors. The ML intensity increases linearly with the increasing the dropping height of the moving piston; that is, the ML intensity depends upon the impact velocity of the moving piston [$v_0 = \sqrt{2gh}$ (where “g” is the acceleration due to gravity and “h” is the height through which the load is dropped freely)]. The ML intensity of $\text{Sr}_2\text{MgSi}_2\text{O}_7:\text{Eu}^{3+}$ and $\text{Sr}_2\text{MgSi}_2\text{O}_7:\text{Eu}^{3+}$, R^+ phosphors were increases linearly with increasing the mechanical stress. Increasing impact velocity causes more number of Eu^{3+} ions to get excited to the higher energy level, subsequently de-excitation of more Eu^{3+} ions occurs. This gives rise to increase in ML intensity [36].

However, from the ML glow curve, ML intensities are different for the different phosphors [see Fig. 9a–d, 10]. The strongest ML intensity could be obtained in the order of $\text{Sr}_2\text{MgSi}_2\text{O}_7:\text{Eu}^{3+}$, $\text{Li}^+ \gg \text{Sr}_2\text{MgSi}_2\text{O}_7:\text{Eu}^{3+}$, $\text{Na}^+ \gg \text{Sr}_2\text{MgSi}_2\text{O}_7:\text{Eu}^{3+}$, $\text{K}^+ \gg \text{Sr}_2\text{MgSi}_2\text{O}_7:\text{Eu}^{3+}$ phosphors.

Figure 11 shows the dependence of peak ML intensities on impact velocity of prepared $\text{Sr}_2\text{MgSi}_2\text{O}_7:\text{Eu}^{3+}$, Li^+ ; $\text{Sr}_2\text{MgSi}_2\text{O}_7:\text{Eu}^{3+}$, Na^+ ; $\text{Sr}_2\text{MgSi}_2\text{O}_7:\text{Eu}^{3+}$, K^+ ; $\text{Sr}_2\text{MgSi}_2\text{O}_7:\text{Eu}^{3+}$ phosphors. The ML intensity of prepared phosphors was increases with increasing the mechanical stress. The $\text{Sr}_2\text{MgSi}_2\text{O}_7:\text{Eu}^{3+}$, Li^+ phosphor possess the strongest ML intensity as compare to other prepared $\text{Sr}_2\text{MgSi}_2\text{O}_7:\text{Eu}^{3+}$, Na^+ ; $\text{Sr}_2\text{MgSi}_2\text{O}_7:\text{Eu}^{3+}$, K^+ ; $\text{Sr}_2\text{MgSi}_2\text{O}_7:\text{Eu}^{3+}$ phosphors [37].

The relationship between semi-log plot of ML intensity versus $(t-t_m)$ for $\text{Sr}_2\text{MgSi}_2\text{O}_7:\text{Eu}^{3+}$ and $\text{Sr}_2\text{MgSi}_2\text{O}_7:\text{Eu}^{3+}$, R^+ phosphors were shown in Fig. 12a–d and the lines were fitted using the Eq. (6) with Origin Pro 8.0

$$\tau = \frac{1}{\text{slope of straight line}} \tag{6}$$

Curve fitting results show that decay constant (τ) varies from 1.47 to 0.85 ms. The ML decay constant value was decreases with the impact velocities, and maximum for the minimum impact velocities (See Table 3). In order to further clarification of the ML decay mechanism in $\text{Sr}_2\text{MgSi}_2\text{O}_7:\text{Eu}^{3+}$ and $\text{Sr}_2\text{MgSi}_2\text{O}_7:\text{Eu}^{3+}$, R^+ phosphors, more experimental and theoretical studies were needed.

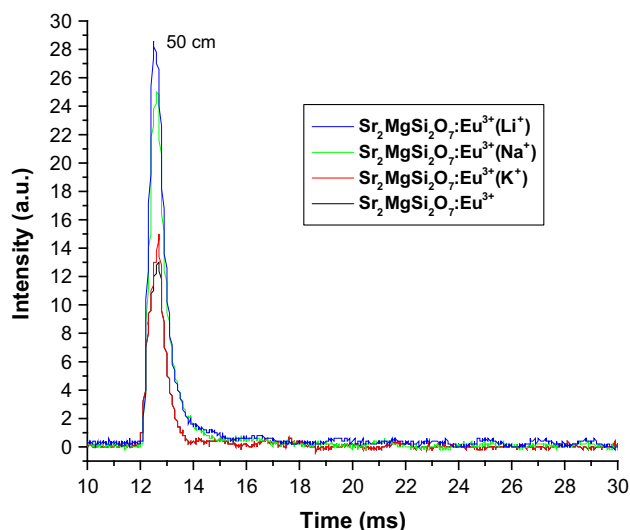


Fig. 10 Comparative ML intensity versus time of $\text{Sr}_2\text{MgSi}_2\text{O}_7:\text{Eu}^{3+}$ and $\text{Sr}_2\text{MgSi}_2\text{O}_7:\text{Eu}^{3+}$, R^+ phosphors

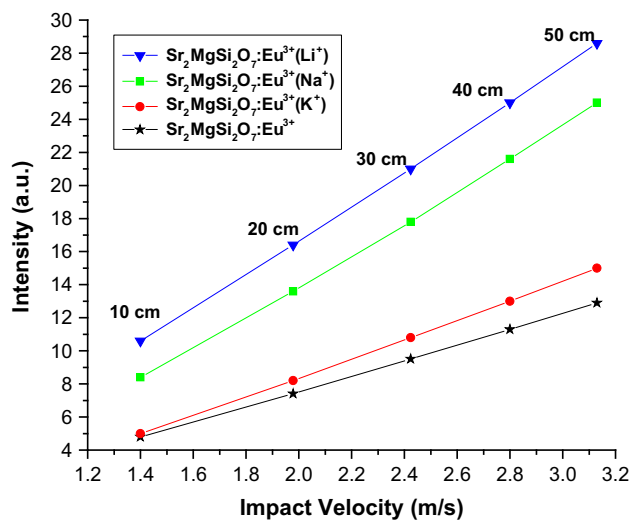


Fig. 11 Comparative ML intensity versus impact velocity of $\text{Sr}_2\text{MgSi}_2\text{O}_7:\text{Eu}^{3+}$ and $\text{Sr}_2\text{MgSi}_2\text{O}_7:\text{Eu}^{3+}$, R^+ phosphors

When a mechanical stress, such as compression, friction, and striking, and so on, was applied onto the sintered $\text{Sr}_2\text{MgSi}_2\text{O}_7:\text{Eu}^{3+}$ and $\text{Sr}_2\text{MgSi}_2\text{O}_7:\text{Eu}^{3+}$, R^+ phosphors, piezo-electric field can be produced [38, 39]. Therefore, in such phosphors the ML excitation may be caused by the local piezoelectric field near the impurities and defects in the crystals. During the impact on the material, one of its newly created surfaces gets positively charged and the other surface of the crack gets negatively charged (Fig. 13). Thus, an intense electric field in the order of 10^6 – 10^7 V/cm is produced [40]. Under such order of electric field, the ejected electrons from the negatively charged surface may be accelerated and subsequently their impact

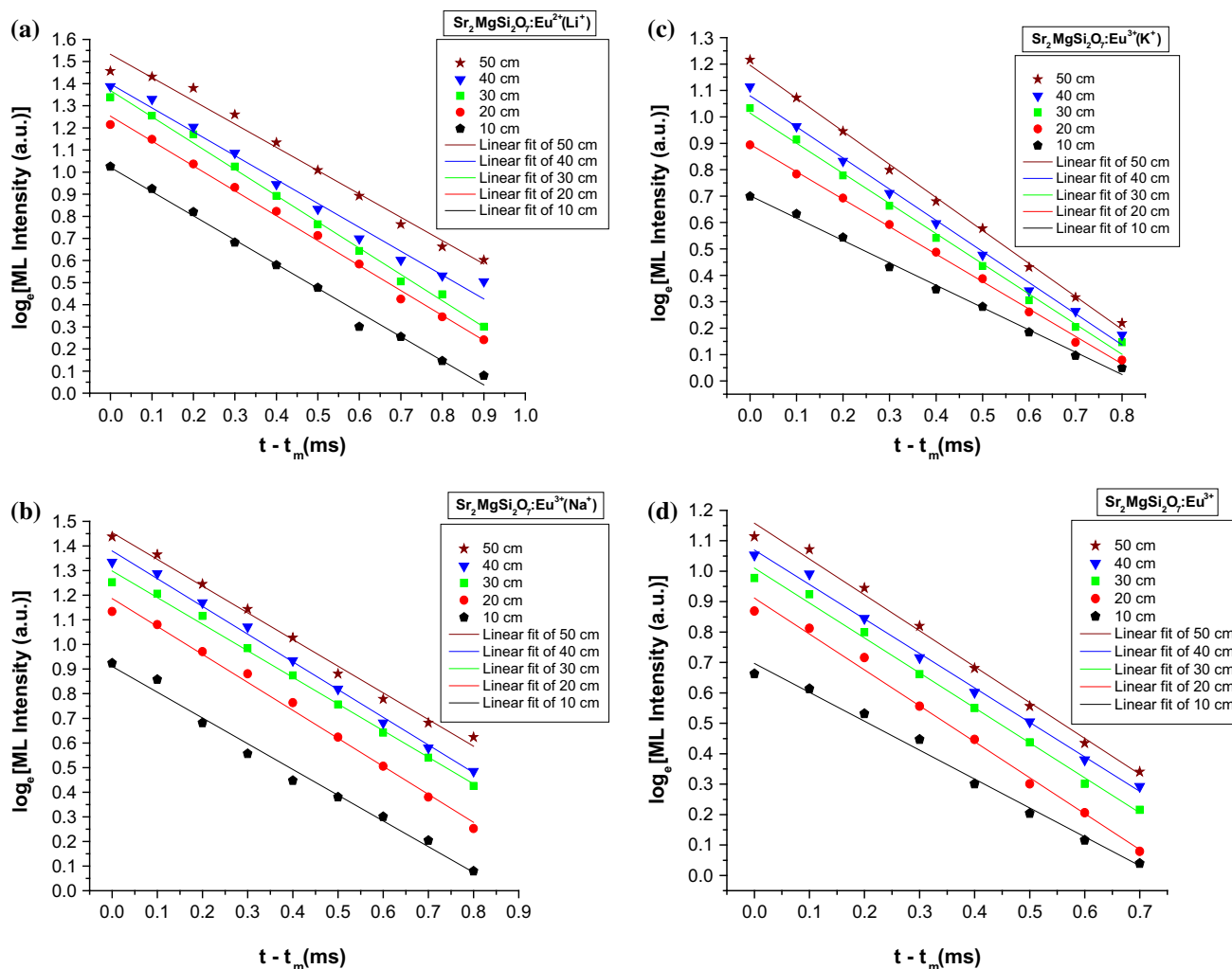


Fig. 12 **a** Semi-log plot of ML intensity versus $(t - t_m)$ for $\text{Sr}_2\text{MgSi}_2\text{O}_7:\text{Eu}^{3+}$, Li^+ phosphor. **b** Semi-log plot of ML intensity versus $(t - t_m)$ for $\text{Sr}_2\text{MgSi}_2\text{O}_7:\text{Eu}^{3+}$, Na^+ phosphor. **c** Semi-log plot

of ML intensity versus $(t - t_m)$ for $\text{Sr}_2\text{MgSi}_2\text{O}_7:\text{Eu}^{3+}$, K^+ phosphor. **d** Semi-log plot of ML intensity versus $(t - t_m)$ for $\text{Sr}_2\text{MgSi}_2\text{O}_7:\text{Eu}^{3+}$ phosphor

Table 3 Calculation of ML decay constant

Impact velocity	10 cm	20 cm	30 cm	40 cm	50 cm
τ Decay constant (ms) $\text{Sr}_2\text{MgSi}_2\text{O}_7:\text{Eu}^{3+}$	1.05	0.84	0.87	0.88	0.79
τ Decay constant (ms) $\text{Sr}_2\text{MgSi}_2\text{O}_7:\text{Eu}^{3+}$ (K^+)	1.19	0.97	0.88	0.85	0.80
τ Decay constant (ms) $\text{Sr}_2\text{MgSi}_2\text{O}_7:\text{Eu}^{3+}$ (Na^+)	0.95	0.88	0.93	0.89	0.81
τ Decay constant (ms) $\text{Sr}_2\text{MgSi}_2\text{O}_7:\text{Eu}^{3+}$ (Li^+)	0.92	0.88	0.84	0.93	0.95

on the positively charged surfaces may excite the luminescence center. Thus, depending on the prevailing conditions, recombination luminescence may be produced. For the impact velocity, the impact pressure P_0 will be equals to, $P_0 = Zv_0$, where Z is a constant [41]. With increasing value of impact velocity, the trap depth will decrease, therefore, for the trap depth beyond a particular pressure the traps will be unstable and they will be de-trapped, in which the number of de-trapped electrons will increases

with the increasing impact velocity. Thus, the ML intensity will increase proportionally with increasing value of impact velocity [42].

As the impact velocity increases, the impact pressure also increases leading to the increase in the electric field at local region which causes the decrease in trap depth. Hence the probability of de-trapping increases [43]. From Fig. 9 inset and 11, it can be seen that with increasing impact velocity, ML intensity also increases linearly i.e., the ML

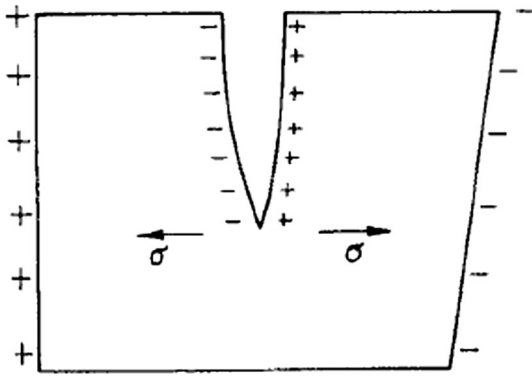


Fig. 13 Langevin model for the piezo-electrification induce phosphor

intensity of $\text{Sr}_2\text{MgSi}_2\text{O}_7:\text{Eu}^{3+}$ and $\text{Sr}_2\text{MgSi}_2\text{O}_7:\text{Eu}^{3+}$, R^+ phosphors are linearly proportional to the magnitude of the impact velocity. When the surface of an object was coated with the ML materials, the stress distribution in the object beneath the layer could be reflected by the ML brightness and could be observed. Based on the above analysis these phosphors can also be used as sensors to detect the stress of an object [44, 45].

4 Conclusion

In summary, $\text{Sr}_2\text{MgSi}_2\text{O}_7:\text{Eu}^{3+}$ and $\text{Sr}_2\text{MgSi}_2\text{O}_7:\text{Eu}^{3+}$, R^+ ($\text{R}^+ = \text{Li}^+$, Na^+ and K^+) phosphors were synthesized by high temperature solid state reaction method at 1200 °C and its luminescence properties were investigated. The tetragonal crystallographies of prepared phosphors were confirmed by the XRD. PL measurements showed that the prepared phosphors exhibited emission peak with good intensity at 590 and 614 nm, corresponding to strong $^5\text{D}_0 \rightarrow ^7\text{F}_1$ orange emission and weak $^5\text{D}_0 \rightarrow ^7\text{F}_2$ red emission. The excitation band at 395 nm can be assigned to $^7\text{F}_0 \rightarrow ^5\text{L}_6$ transition of Eu^{3+} ions due to the typical f–f transitions. CIE color chromaticity diagram confirms the prepared $\text{Sr}_2\text{MgSi}_2\text{O}_7:\text{Eu}^{3+}$ and $\text{Sr}_2\text{MgSi}_2\text{O}_7:\text{Eu}^{3+}$, R^+ phosphors exhibits orange-red emission, indicating that it has favorable properties for application as near ultraviolet LED conversion phosphor. The phosphorescent life time of $\text{Sr}_2\text{MgSi}_2\text{O}_7:\text{Eu}^{3+}$, Li^+ phosphor can be calculated by a curve fitting technique, and the decay curves fitted by the sum of two exponential components have different decay times ($\tau_1 = 1.33$ ms; $\tau_2 = 76.86$ ms) and they possess the fast and slow decay process. It is worthy to note that the dependence between ML intensity of prepared $\text{Sr}_2\text{MgSi}_2\text{O}_7:\text{Eu}^{3+}$ and $\text{Sr}_2\text{MgSi}_2\text{O}_7:\text{Eu}^{3+}$, R^+ phosphors and the impact velocity of the moving piston is close to linearity, which suggests these phosphors can also be used as sensors to detect the stress of an object. The charge compensator

ions R^+ ($\text{R}^+ = \text{Li}^+$, Na^+ and K^+) in $\text{Sr}_2\text{MgSi}_2\text{O}_7:\text{Eu}^{3+}$ can further enhance luminescence intensity, and the emission intensity of $\text{Sr}_2\text{MgSi}_2\text{O}_7:\text{Eu}^{3+}$ doping Li^+ is higher than that of Na^+ or K^+ .

References

1. H.W. Leverenz, *An Introduction to Luminescence of Solids* (Dover Publications Inc., New York, 1968)
2. H. Wu, Y. Hu, Y. Wang, B. Zeng, Z. Mou, L. Deng, W. Xie, J. Alloys Compd. **486**, 549 (2009)
3. I.P. Sahu, D.P. Bisen, N. Brahme, J. Biol. Chem. Lumin. **30**(7), 1125 (2015)
4. F.W. Kang, Y. Hu, L. Chen, X.J. Wang, H. Wu, Z. Mu, J. Lumin. **135**, 113 (2013)
5. Z. Song, J. Liao, X. Ding, T. Zhou, Q.L. Liu, J. Lumin. **132**, 1768 (2012)
6. Y. Zhai, Q. Zhao, Y. Han, M. Wang, J. Yu, J. Mater. Sci. Mater. Electron. **27**(1), 677 (2016)
7. X. Dong, J. Zhang, X. Zhang, Z. Hao, Y. Luo, J. Alloys Compd. **587**, 493 (2014)
8. J. Zheng, Q. Cheng, W. Chen, Z. Guo, C. Chen, J. Solid State Sci. Technol. **4**(5), R72 (2015)
9. I.P. Sahu, D.P. Bisen, N. Brahme, Res. Chem. Intermed. **41**(9), 6649 (2015)
10. S. Kamei, Y. Kojima, N. Nishimiya, J. Lumin. **130**, 2247 (2010)
11. I.P. Sahu, D.P. Bisen, N. Brahme, L. Wanjari, R.K. Tamrakar, Res. Chem. Intermed. **41**, 8797 (2015)
12. M. Xu, L. Wang, L. Liu, D. Jia, R. Sheng, J. Lumin. **146**, 475 (2014)
13. I.P. Sahu, J. Mater. Sci. Mater. Electron. **26**(9), 7059 (2015)
14. B.P. Chandra, J. Lumin. **131**, 1203 (2011)
15. C.N. Xu, C. Li, Y. Imai, H. Yamada, Y. Adachi, K. Nishikubo, Adv. Sci. Technol. **45**, 939 (2006)
16. I.P. Sahu, D.P. Bisen, R.K. Tamrakar, R. Shrivastava, Res. Chem. Intermed. **42**(3), 1823 (2016)
17. JCPDS file number 75-1736, JCPDS International Center for Diffraction Data
18. I.P. Sahu, D.P. Bisen, N. Brahme, R.K. Tamrakar, J. Lumin. **167**, 278 (2015)
19. Z. Zhang, Y. Wang, H. Wang, Z. Sun, L. Jia, J. Phys: Conf. Ser. **152**, 012050 (2009)
20. Z. Yuan, C. Chang, D. Mao, W.J. Ying, J. Alloys Compd. **377**(1–2), 268 (2004)
21. I.P. Sahu, D.P. Bisen, N. Brahme, R.K. Tamrakar, J. Mater. Sci. Mater. Electron. **26**, 10075 (2015)
22. H.B. Premkumar, H. Nagabhushana, S.C. Sharma, S.C. Prashantha, H.P. Nagaswarupa, B.M. Nagabhushana, R.P.S. Chakradhar, J. Alloys Compd. **601**, 75 (2014)
23. V. Pagonis, G. Kitis, C. Furetta, *Numerical and Practical Exercises in Thermoluminescence* (Springer, Berlin, 2006)
24. R. Chen, S.W.S. McKeever, *Theory of Thermoluminescence and Related Phenomenon* (World Scientific Press, Singapore, 1997)
25. C. Devayani, S.K. Omanwar, S.V. Moharil, J. Lumin. **142**, 180 (2013)
26. G. Vicentini, L.B. Zinner, J. Zukerman-Schpector, K. Zinner, Coord. Chem. Rev. **196**, 353 (2000)
27. H.Y. Jiao, Y. Wang, Phys. B **407**, 2729 (2012)
28. H. Nagabhushana, D.V. Sunitha, S.C. Sharma, B.D. Prasad, B.M. Nagabhushana, R.P.S. Chakradhar, J. Alloys Compd. **595**, 192 (2014)

29. H. Liu, Y. Hao, H. Wang, J. Zhao, P. Huang, B. Xu, J. Lumin. **131**, 2422 (2011)
30. I.P. Sahu, D.P. Bisen, N. Brahme, R.K. Tamrakar, R. Shrivastava, J. Mater. Sci. Mater. Electron. **26**, 9907 (2015)
31. CIE (1931) International Commission on Illumination. Publication CIE no. 15 (E-1.3.1)
32. I.P. Sahu, D.P. Bisen, N. Brahme, R.K. Tamrakar, J. Radiat. Res. Appl. Sci. **8**, 104 (2015)
33. T. Aitasalo, P. Daren, J. Holsa, K. Junger, J.C. Krupa, M. Lastusaari, J. Legendziewicz, J. Niittykoski, W. Strek, J. Solid State Chem. **171**, 114 (2003)
34. D.R. Vij, *Luminescence of Solids* (Plenum Press, New York, 1998)
35. I.P. Sahu, D.P. Bisen, N. Brahme, R.K. Tamrakar, J. Mater. Sci. Mater. Electron. **27**(2), 1828 (2016)
36. B.P. Chandra, Open Nanosc. J. **5**, 45 (2011)
37. I.P. Sahu, D.P. Bisen, N. Brahme, Lumin. J. Biol. Chem. Lumin. **30**(5), 526 (2015)
38. I.P. Sahu, P. Chandrakar, R.N. Baghel, D.P. Bisen, N. Brahme, R.K. Tamrakar, J. Alloys Compd. **649**, 1329 (2015)
39. H. Zhang, N. Terasaki, H. Yamada, C.N. Xu, Thin Solid Films **518**, 610 (2009)
40. I.P. Sahu, D.P. Bisen, N. Brahme, J. Radiat. Res. Appl. Sci. **8**, 381 (2015)
41. X. Wang, C.N. Xu, H. Yamada, K. Nishikubo, X.G. Zheng, Adv. Mater. **17**, 1254 (2005)
42. I.P. Sahu, D.P. Bisen, N. Brahme, Displays **38**, 68 (2015)
43. H. Zhang, N. Terasaki, H. Yamada, C.N. Xu, Int. J. Modern Phys. B **23**, 1028 (2009)
44. H. Zhang, C.N. Xu, N. Terasaki, H. Yamada, Phys. E **42**, 2872 (2010)
45. I.P. Sahu, D.P. Bisen, N. Brahme, Displays **35**, 279 (2014)